Formation, growth, and saturation of dry holes in thick liquid films under vapor-mediated Marangoni effect

Cite as: Phys. Fluids **31**, 112105 (2019); https://doi.org/10.1063/1.5127284
Submitted: 10 September 2019 . Accepted: 01 November 2019 . Published Online: 14 November 2019

Seungho Kim, Joonoh Kim, and Ho-Young Kim

Physics of Fluids ARTICLE scitation.org/journal/phf

Formation, growth, and saturation of dry holes in thick liquid films under vapor-mediated Marangoni effect

Cite as: Phys. Fluids 31, 112105 (2019); doi: 10.1063/1.5127284
Submitted: 10 September 2019 • Accepted: 1 November 2019 •
Published Online: 14 November 2019

Seungho Kim,[1,2,a)] Joonoh Kim,[1,a)] and Ho-Young Kim[1,b)]

AFFILIATIONS

[1] Department of Mechanical and Aerospace Engineering, Seoul National University, Seoul 08826, South Korea
[2] Department of Biological and Environmental Engineering, Cornell University, Ithaca, New York 14853, USA

[a)] **Contributions:** S. Kim and J. Kim contributed equally to this work.
[b)] **Electronic mail:** hyk@snu.ac.kr

ABSTRACT

Films and drops of liquids can change their shapes and move under the spatial gradient of surface tension. A remote volatile liquid of relatively low surface tension can induce such flows because its vapor locally lowers the surface tension of the films and drops. Here, we show that aqueous liquid films thicker than approximately 100 μm can be punctured to immediately expose a dry hole by an overhanging isopropyl alcohol drop, which is attributed to the vapor-mediated Marangoni effect. We construct and corroborate scaling laws to predict the film dynamics, considering the balance of the driving capillary force and resisting viscous and hydrostatic forces as well as the contact angle of the alcohol-adsorbed solid surface. This remote scheme to induce and sustain changes of liquid morphology can be applied for fluid sculpture and patterning for industrial and artistic practices.

I. INTRODUCTION

Liquid films on nonwettable solid surfaces are unstable if they thin below a critical thickness which is determined by the surface tension of the liquid, wettability (or contact angle), and gravity.[1] Small disturbances can nucleate a dry hole in such films, and the hole expands *spontaneously* over time by forming a ridge around the rim as a result of liquid accumulation. The growth dynamics of the hole, driven by the capillarity to minimize the surface free energy and resisted by viscous and gravitational forces, can be mainly classified by the relative importance of the inertia. In an inertia-dominated regime, the radius of the dry hole, r, was shown to grow like $r \sim t$ with t being time, whose proportionality constant involves the well-known Taylor-Culick retraction velocity of a liquid sheet, $\sqrt{2\gamma/(\rho h)}$.[2–4] Here, γ and ρ denote the liquid-gas surface tension coefficient and the density of the liquid, respectively, and h is the film thickness. In a viscosity-dominated regime, we still have $r \sim t$ but with the constant retraction velocity involving the viscosity as well as the surface tension.[1] Different power laws can arise if the film thickness is so small that the slipping effects or intermolecular forces are no longer negligible.[5,6]

Unlike those liquid films on nonwettable solids exhibiting spontaneous dewetting, liquid films on highly wettable solid surfaces can retract from the solids via external stimuli including air blowing[7] and mixing with a low surface tension liquid.[8–11] In particular, the gradient of liquid-gas surface tension owing to the addition of the low surface tension liquid gives rise to the Marangoni stress that pushes the liquid away from the region of a low surface tension. Similar Marangoni stress can arise by placing a drop of volatile organic liquid near the liquid drops of a relatively higher surface tension. In this case, the local adsorption or absorption of vapor molecules can lead to the spatial variation of the surface tension. Such a vapor-mediated Marangoni effect was used to propel liquid drops away from the vapor source[12–16] and to suppress the so-called coffee ring effect by creating mixing flows within evaporating drops.[17–19] It was shown that a hole can form in a so-called Savart sheet placed underneath a drop of a volatile organic liquid.[20] The contact angle of a sessile drop of the binary liquid mixture was found to change due

to uneven evaporation rates of its components, which generates the Marangoni stress.[21]

The dewetting of a liquid film on wettable surfaces due to a volatile drop placed nearby was used to promote liquid drying and solid surface cleaning.[22–25] Recently, it was shown that aqueous films of thickness on the order of 10 μm undergo dewetting by leaving a very thin liquid layer when an alcohol drop is situated above the film.[26] While the bulk film recedes on the underlying thin layer with the inner radius of the bulk ridge r_b growing like $t^{1/2}$, the thin layer is dried to expose a dry hole whose radius grows like $t^{2/3}$. Here, we report novel liquid film dynamics that emerge when the thickness of aqueous films exceeds ~100 μm, referred to as *thick* films here, under the vapor-mediated Marangoni effect caused by an overhanging IPA (isopropyl alcohol) drop. The thin layer under the receding bulk is absent, allowing us to observe the receding bulk directly exposing a central dry hole. Unlike the aforementioned holes resulting from the film dewetting, the hole radius grows like t initially but changes its power law to $t^{1/2}$ and then eventually reaches a plateau. We present the visualization results of the film dynamics and theoretically rationalize the observed power laws. We find that the change of the interfacial tension of the solid due to the adsorption of IPA molecules plays an important role in the dynamics of dry holes of thick liquid films.

II. EXPERIMENTAL

To prepare a wettable solid surface, we treat a Si wafer 10 cm in diameter with piranha solution and oxygen plasma. As film liquids, we use deionized water (liquid A) and aqueous glycerine of 30 wt. % (liquid B). The density (ρ), the surface tension coefficient (γ_0), and the viscosity (μ) of the liquids at 25 °C are such that ρ = 998 kg m^{-3}, γ_0 = 72 mN m^{-1}, and μ = 1 mPa s for water and ρ = 1071 kg m^{-3}, γ_0 = 69 mN m^{-1}, and μ = 2.2 mPa s for the aqueous glycerine. The thickness of the liquid film on the solid surface, h_0, is deduced from the weight measurement by a precision balance (Mettler Toledo XS205), whose resolution is 0.1 mg, corresponding to the thickness uncertainty range of ±0.01 μm. As a source of IPA vapor, a glass capillary tube of inner radius a = 0.58 mm filled with liquid IPA is situated at a vertical distance of d from the film surface. A CMOS (complementary metal-oxide-semiconductor) camera (Photron SA 1.1) images the film shapes.

Figures 1(a) and 1(b) show the temporal evolutions of the liquid films of 260 μm and 50 μm thickness, respectively. We find drastic differences between the dynamic behaviors of thick and thin films. The cross section of the film in each case is schematically illustrated in Figs. 1(c) and 1(d). Because the IPA vapor concentration is higher just beneath the capillary, the liquid-gas interfacial tension in the

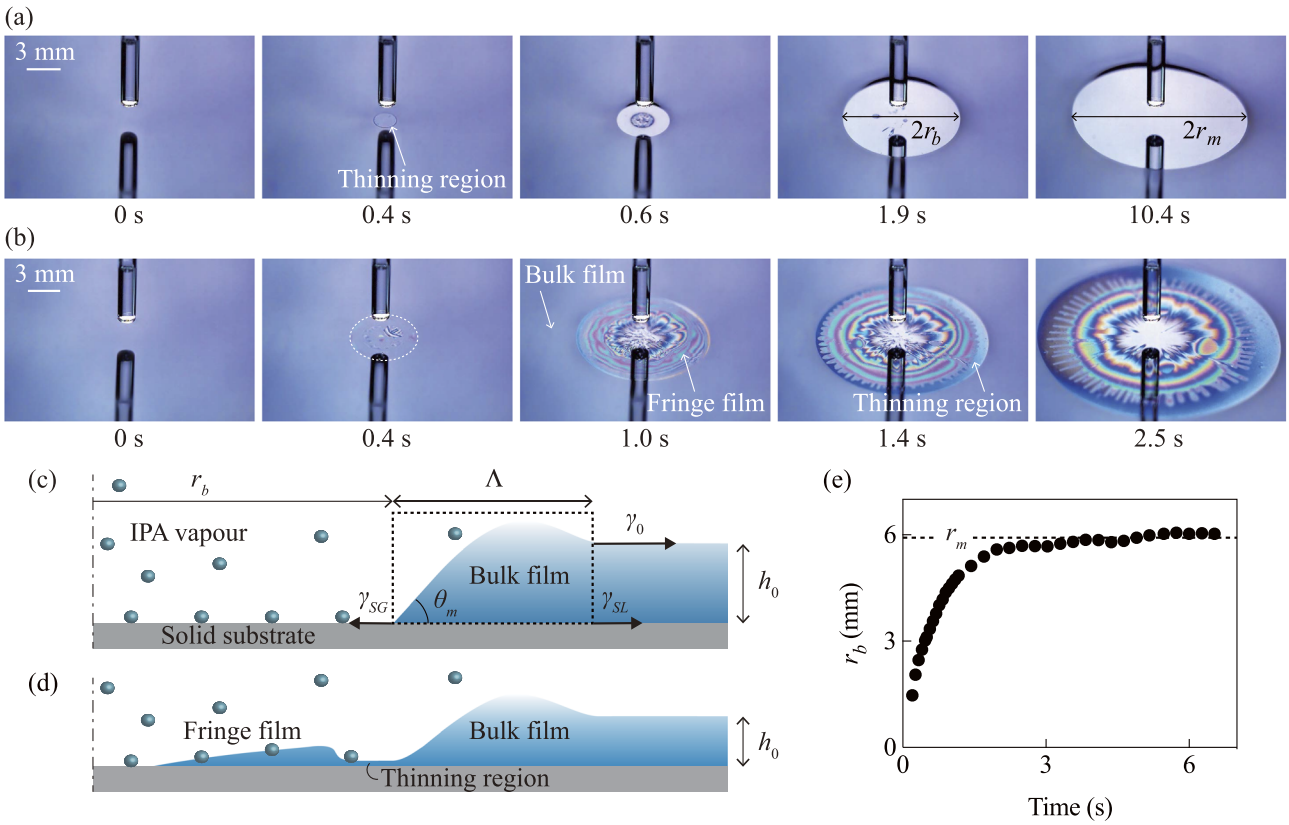

FIG. 1. Temporal evolutions of the morphology of water films with the original thickness (a) h_0 = 260 μm and (b) h_0 = 50 μm due to IPA vapor from the source in an overhanging capillary. (c) Schematic of the cross section of the dewetting thick film as shown in (a). (d) Schematic of the cross section of the thin film as shown in (b). (e) Temporal evolution of the inner radii of bulk film r_b of a water film with h_0 = 320 μm.

center is lower than that in the periphery, leading to the radially outward Marangoni flow. In the relatively thin film in Fig. 1(b), the receding bulk leaves a thin liquid layer in the center, which is punctured by evaporation. The thin layer is called a fringe film, and it is connected to the rim of bulk via a narrow region of further reduced thickness, called a thinning region. While thin films with $h_0 \sim 10\ \mu$m exhibit the development of those distinct regions over 1 s, relatively thick films with $h_0 > 100\ \mu$m show rapid drying of a thinning region, which first appears at 0.4 s in Fig. 1(a). The thinning region occurs where too much liquid flows from the central film to receding bulk as the advection (and thus dilution) rate of IPA into bulk overwhelms the diffusion rate of IPA from the atmosphere.[26] For thicker films, the advection rate is higher (thanks to the reduced viscous friction), thereby causing the thinning region to occur earlier. Our experiments reveal that when the film thickness exceeds ~100 μm, the bulk recession is so vigorous just beneath the IPA source that the thinning region generated extremely early turns to a dry region rapidly, as shown in the images at $t = 0.4$ and 0.6 s in Fig. 1(a). The dry area initially contains a central liquid island or a residual fringe film which is completely dried by 1.9 s, and then, the dry circular area further grows.

Figure 1(c) shows the film profile after the initial transient of central film evaporation, where the ridge of bulk starting at r_b extends by a characteristic length Λ before joining a bulk film of original thickness h_0. We show typical experimental measurement data of r_b vs time in Fig. 1(e), where the initially growing hole radius is saturated to a steady value. As mentioned above, we focus on the temporal evolution of thick films corresponding to Fig. 1(a), which is in contrast with the thin film dynamics which were analyzed previously.[26]

We note that the recession of the bulk film arises on a dry solid surface which continually meets IPA vapor molecules that can change the solid surface energy. Thus, characterizing the wettability of the exposed solid surface under the effects of atmospheric IPA vapor is important in order to understand the dynamics of the receding bulk film. We quantify the interfacial tension of the IPA-exposed solid surface in the Appendix. In Secs. III A and III B, we move on to theoretically discuss the rate of the hole growth and the maximum hole radius.

III. THEORETICAL ANALYSIS

A. Growth of dry hole

While thin films recede leaving a central fringe film [Fig. 1(b)] under the effect of the surrounding IPA vapor, thick films recede without trails, i.e., they move on a dry surface as shown in Fig. 1(a). Figure 2(a) plots the experimentally measured radius of the dry hole or the inner radius of bulk, r_b, for various experimental conditions using thick films as listed in Fig. 2(e). The inset of Fig. 2(a) shows the representative data of r_b of liquids A and B in the log-log scale to show that it grows linearly with time t initially and then changes its trend to grow like $t^{1/2}$ before it plateaus. This behavior is distinguished from the receding dynamics of bulk in thin films as previously studied,[26] where r_b increases like $t^{1/2}$ from the beginning.

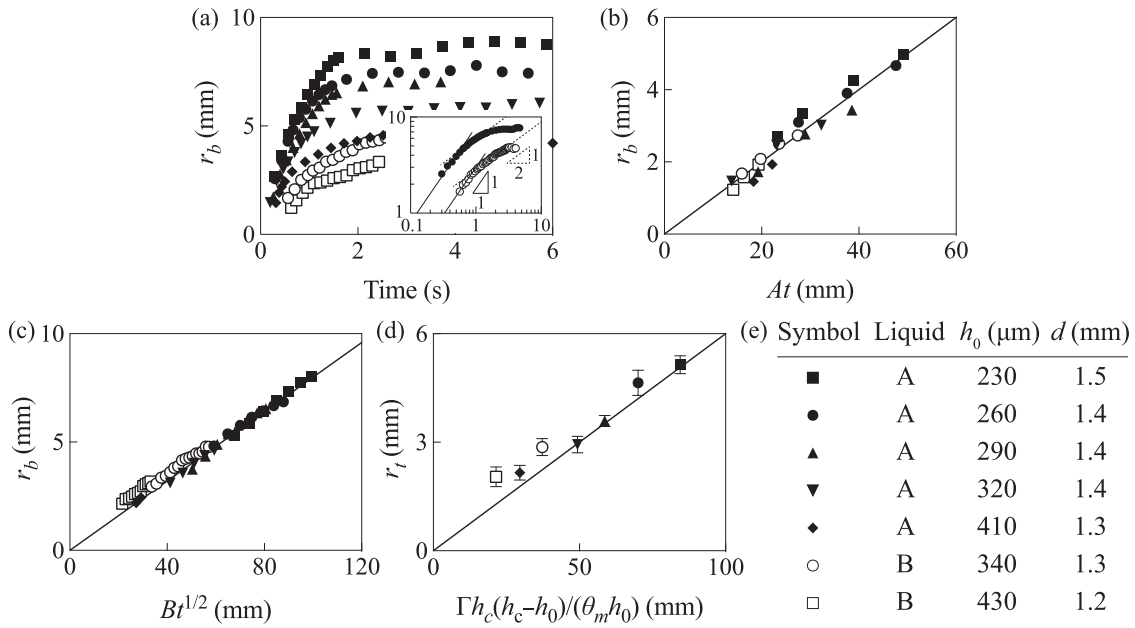

FIG. 2. (a) The experimentally measured radius of a dry hole, r_b, vs time, t. Inset: the log-log plot of the representative data of r_b vs t. (b) r_b in the early stages, plotted according to scaling law (1) with $A = \rho g\theta_m\left(l_c^2\theta_m^2 - h_0^2\right)/(\mu\Gamma)$. The slope of the best fitting line is 0.1. (c) r_b in the late stages, plotted according to scaling law (2) with $B = (h_c - h_0)l_c^{-1}[\gamma_0 h_c(h_c/h_0 + 1)/\mu]^{1/2}$. The slope of the best-fitting line is 0.08. (d) Transition radius for the receding rate, plotted according to scaling law (3). The slope of the best fitting line is 0.06. (e) Experimental conditions for the symbols.

To understand the initial constant-velocity regime, we consider forces acting on a black-dotted control volume in Fig. 1(c), where we ignore the curvature effect for $h_0 \ll r_b$. The imbalance of interfacial tensions gives rise to the driving force per unit depth for the bulk receding: $F_d = \gamma_0 - (\gamma_{SG} - \gamma_{SL})$. Here, we assume that the liquid-gas interfacial tension of the bulk surface beyond the ridge is close to the uncontaminated value owing to continual replenishing flows. Our measurement results of the solid interfacial tensions in the Appendix allow us to write $\gamma_{SG} - \gamma_{SL} = \gamma_0 \cos\theta_m$, where θ_m is the receding contact angle of the bulk film as shown in Fig. 1(c). For $\theta_m \ll 1$, we get $F_d \approx \gamma_0\theta_m^2/2$.

The recession of bulk is resisted by viscous shear and hydrostatic forces. Here, we neglect inertial effects because $\mathrm{Re}(h_0/r_b) \ll 1$,[27] where both the Reynolds number, $\mathrm{Re} = \rho\dot{r}_b h_0/\mu$, and h_0/r_b are on the order of 10^{-1}. For inertialess flows in the wedge of bulk with a thickness profile of $z = h(x)$ with $h(0) = 0$ at the contact line, the velocity field is given by $u(x, z) = 3\dot{r}_b z(h - z/2)/h^2$. The viscous shear force over the area ranging from $x = 0$ to Λ is written as $F_v = \int_0^\Lambda \tau \mathrm{d}x$ with the wall shear stress $\tau = \mu(\mathrm{d}u/\mathrm{d}z)|_{z=0}$. Considering that the shear stress near the contact line dominates the integral and approximating $h \approx x\theta_m$, we estimate $F_v \approx 3\mu\dot{r}_b \ln(\Lambda/\lambda)/\theta_m$, where the cutoff length of a molecular scale, λ, has been introduced to relieve singularity. Therefore, the resisting force per unit depth, $F_r = F_v + \frac{1}{2}\rho g h_0^2$, where the second term in the right-hand side corresponds to the hydrostatic force.

Balancing F_d and F_r gives a constant velocity of bulk dewetting $\dot{r}_b \sim (\gamma_0\theta_m^2 - \rho g h_0^2)\theta_m/(\mu\Gamma)$ with $\Gamma = \ln(\Lambda/\lambda)$. Hence, r_b increases linearly with t as

$$r_b \sim \frac{\rho g \theta_m}{\mu\Gamma}\left(l_c^2\theta_m^2 - h_0^2\right)t, \tag{1}$$

where $l_c = \sqrt{\gamma_0/(\rho g)}$ is the capillary length. The logarithmic value, Γ, is rather insensitive to a precise value of Λ, which is experimentally found to be maintained almost constant (3 mm) in the early stages, regardless of the experimental conditions, and λ is taken to be 1 nm in this work. Figure 2(b) shows that the experimental data of r_b in the early stages under various conditions as listed in Fig. 2(e) are collapsed onto a single line when plotted according to scaling law (1).

As the bulk keeps receding, the liquid displaced from the central region accumulates in the rim, which grows so large that its height reaches the critical height, h_c. It is determined by the balance between the hydrostatic force, $\frac{1}{2}\rho g h_c^2$, and the interfacial tension imbalance, $\gamma_0 + \gamma_{SL} - \gamma_{SG}$,[1] so that $h_c \approx l_c\theta_m$ for $\theta_m \ll 1$. The physical properties of the liquids used in this work give $h_c = 710$ and 670 μm for liquids A and B, respectively, with $\theta_m = 15°$ for both the liquids. As the flattened rim of height h_c grows in its radial extension owing to the bulk receding, the viscous dissipation in the flat region dominates over the wedge dissipation.[28] Then, the viscous shear force per unit depth acting on the flattened rim of the characteristic extension Λ' is given by $F_v \approx 3\mu\dot{r}_b\Lambda'/h_c$. Here, $\Lambda' \approx \frac{1}{2}h_0 r_b/(h_c - h_0)$ results from the mass conservation.

With the same expressions for the driving and hydrostatic forces as in the early stages, balancing F_d and F_r yields a scaling law for r_b in the late stages,

$$r_b \sim \frac{h_c - h_0}{l_c}\left[\frac{\gamma_0}{\mu}h_c\left(\frac{h_c}{h_0} + 1\right)\right]^{1/2} t^{1/2}. \tag{2}$$

Figure 2(c) shows that our theory is consistent with the experiment in the late stages with the scattered raw data in Fig. 2(a) collapsed onto a single line.

To find the transition boundary of the early stage of dewetting where $r_b \sim t$ and the late stage with $r_b \sim t^{1/2}$, we seek r_b where the dissipations in the wedge and in the flattened rim become comparable. Then, we readily find a scaling relation of r_t, the transition radius of the hole,

$$r_t \sim \frac{\Gamma}{\theta_m}\frac{h_c(h_c - h_0)}{h_0}. \tag{3}$$

Figure 2(d) shows that the experimentally obtained transition radii under various conditions are consistent with our theory.

B. Maximum hole radius

As experimentally measured in Fig. 2(a), the hole ceases to grow beyond the late stages of bulk receding but rather keeps a constant radius of r_m. The IPA vapor concentration at this distance from the IPA source is so low that the Marangoni stress is unable to retract the rim of bulk further. Accordingly, r_m corresponds to the location where the Marangoni stress acting on the rim interface is balanced by the hydrostatic pressure. While the rim bulges to form a ridge behind the receding contact line, the film is now flat behind the stalled contact line as shown in the image at $t = 10.4$ s of Fig. 1(a). It is because the high pressure in the ridge leads to its flattening for pressure equilibration when no liquid is further supplied from the center. Then, the flow field is likely to be developed within the wedge, which gives rise to swirls as illustrated in Fig. 3(a). This implies that adsorbed IPA molecules can be engulfed by the swirling flows, leading to $\gamma_{LG} \approx \gamma_0$ at the flat film. We observed in separate experiments that such swirling flows are confined within a few millimeters from the contact line, consistent with the length scale of the wedge.

Therefore, the Marangoni stress τ_m is established by the gradient of the liquid-gas interfacial tension over the wedge length, $l \approx h_0/\theta_m$: $\tau_m \sim (\gamma_0 - \gamma_{LG})/l$. Balancing this stress with the hydrostatic pressure, $\rho g h_0$, leads to $(\gamma_0 - \gamma_{LG})\theta_m \sim \rho g h_0^2$ at r_m. It is known that γ_{LG} decreases linearly with a ratio of the IPA concentration c to the saturation concentration c_s when it is low ($c/c_s < 0.2$), allowing us to write $\gamma_{LG}/\gamma_0 \sim 1 - \xi c/c_s$ with the prefactor ξ of the order of unity.[26] Solving the diffusion equation of c from a source of radius a, we find $c/c_s \approx a/r_b$, when $t \gg \frac{1}{4}r_b^2/D \sim 1$ s,[26,29] which is the case for the maximum hole radius. Here, $D = 1 \times 10^{-5}$ m^2 s^{-1} is the diffusivity of IPA vapor in air.[30] Using this relationship between c and r_b, the foregoing balance of Marangoni and hydrostatic stresses gives the scaling of r_m, i.e., the maximum value of r_b,

$$\frac{r_m}{a} \sim \theta_m\left(\frac{l_c}{h_0}\right)^2. \tag{4}$$

Figure 3(b) displays the measured maximum steady radius of dry holes under various experimental conditions. While r_m decreases with the original film thickness h_0, it is insensitive to the differences of properties of liquids A and B. Figure 3(c) shows that r_m is inversely proportional to h_0^2 while being independent of the viscosity, validating our theory. Similar values of capillary length l_c and

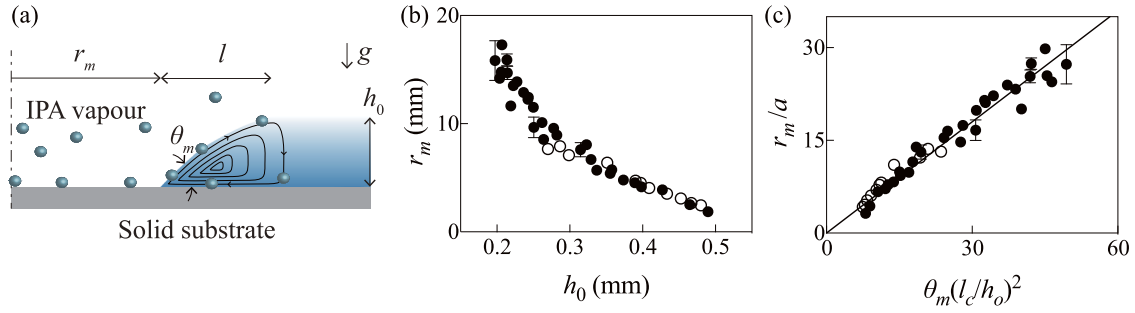

FIG. 3. (a) Schematic of flow field within the wedge when the hole radius reaches its steady maximum. (b) Experimentally measured r_m vs h_0. The filled and empty symbols correspond to liquids A and B, respectively. (c) The experimental data of r_m plotted according to scaling law (4). The slope of the best fitting line is 0.6.

contact angle θ_m of liquids A and B despite the twofold difference in viscosity explain why the raw experimental data tend to lie on the same trend line in Fig. 3(b).

IV. CONCLUSIONS

We have shown that thick aqueous films of the thickness over approximately 100 μm can be punctured to expose a dry hole by an overhanging liquid drop of a relatively low surface tension owing to vapor-mediated Marangoni effects. As the film dewetting involves the motion of the solid-liquid-gas contact line, the interfacial tensions of the solid modified by the adsorption of IPA vapor play an important role in the film dynamics. We have constructed scaling laws to predict the growth rate of the dry hole, considering the balance of the driving capillary force and resisting viscous and hydrostatic forces as well as the contact angle of the IPA-adsorbed solid surface. The morphology change of the rim of the receding bulk was shown to be mainly responsible for the transition of the power law of hole radius from $r_b \sim t$ to $r_b \sim t^{1/2}$. It was revealed that the dry hole ceases to grow at a location where Marangoni and hydrostatic forces are balanced.

The dewetting dynamics of relatively thick films are discriminated from those of relatively thin films in that the receding of the bulk film immediately exposes a central dry hole without leaving a thin layer of liquid, which is called a fringe in dewetting of thin films. Setting up a clear boundary between the two cases is rather impractical as the fringe vanishes gradually with the increase in film thickness. Furthermore, the emergence of the dry hole relies on the evaporation of the layer remaining behind the receding bulk film. If the volatility of the liquid film is lower than the liquids tested in this work, the thinning region was observed to persist without being ruptured. For instance, the dewetting films of aqueous glycerine of 40 wt. % did not expose dry holes for over 100 s in our separate experiments. The precise conditions to lead to the complete evaporation of a thinning region are an important topic to be pursued in the future to further our understanding of Marangoni-driven film dewetting. Such a study will involve the consideration of intermolecular forces between an extremely thin liquid layer (thinner than 100 nm) and a solid surface[31] as well as statistical gas dynamics associated with evaporation. Our experimental finding that a stable liquid film morphology, or a steady hole radius, can be sustained over time via the vapor-mediated Marangoni effect allows us to think about using this scheme for fluid sculpture[32] and patterning[33] for industrial and artistic practices.

ACKNOWLEDGMENTS

This work was supported by the National Research Foundation of Korea (Grant No. 2018-052541) through SNU-IAMD.

APPENDIX: QUANTIFICATION OF SOLID SURFACE ENERGY CHANGE DUE TO IPA VAPOR

As IPA vapor molecules in the atmosphere are adsorbed onto a solid surface, the interfacial energy of the solid changes, which we quantify with a separate experimental setup. A physical parameter of the solid, which is associated with the wetting behavior of the liquid, is the difference between the solid-gas interfacial tension (γ_{SG}) and the solid-liquid interfacial tension (γ_{SL}), as can be seen in Young's equation, $\cos\theta = (\gamma_{SG} - \gamma_{SL})/\gamma_{LG}$. Here, θ is the equilibrium contact angle of a liquid on the solid and γ_{LG} is the liquid-gas interfacial tension.

Figure 4(a) shows an apparatus to measure the contact angle of a sessile drop on a Si wafer under various concentrations of IPA vapor within an acrylic chamber. The chamber with the height of 17 cm and the cross-sectional area of 10 × 10 cm^2 is open to the atmosphere at the top and contains liquid IPA in the bottom. The IPA pool is initially isolated from the air above by a shutter. The Si wafer, measuring 2 × 2 cm^2, is only 6% of the area of the IPA pool; thus, its blockage effect is negligible. Figure 4(b) shows that the contact angle of a water drop, 10 μl in volume, with the solid surface is nearly zero initially. As the IPA concentration in the air increases with time since the shutter is opened, the contact angle θ increases. The temporal evolutions of the contact angle measured at different distances from the IPA pool, s, are plotted in Fig. 4(c). We see that θ increases with time t initially, but it plateaus at $\theta_m \approx 15^\circ$. The plateau appears later as s increases.

Such a change of θ is related to the IPA concentration in the air, c, which was shown to follow the one-dimensional diffusion equation:[26,29] $c = c_s\mathrm{erfc}(\frac{1}{2}s/\sqrt{Dt})$. Here, $c_s = 0.142$ kg m^{-3} and $D = 1 \times 10^{-5}$ m^2 s^{-1} denote the saturation concentration and the diffusivity of IPA vapor in the air, respectively.[30] Figure 4(d) shows

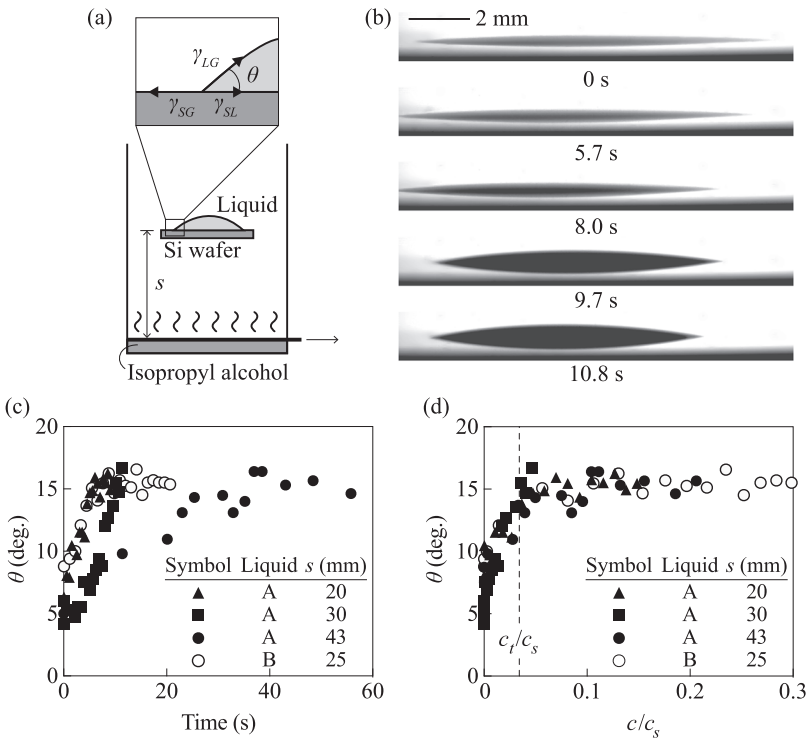

FIG. 4. (a) Experimental apparatus to measure the interfacial tension of the solid under the effects of IPA vapor. (b) Images of a 10 μl water drop on the Si substrate 30 mm above the IPA free surface. As the concentration of IPA vapor in the air increases with time, the contact angle increases. (c) Contact angle of liquid drops on the Si substrates situated various distances from the free surface of IPA pool. (d) Replotting the data of θ vs the scaled concentration of IPA vapor in the air, c/c_s.

that the scattered data of θ are collapsed onto a single curve when plotted vs c/c_s. This implies a dominant effect of the IPA vapor concentration on the contact angle. The contact angle rapidly increases with c initially, but it saturates beyond a critical concentration, $c_t \approx 0.03c_s$, indicated as a dotted line.

Young's equation implies that the increase in θ with the increase in IPA concentration is caused by the decrease in $\gamma_{SG} - \gamma_{SL}$ or the increase in γ_{LG}. It is highly likely that the adsorption of IPA molecules on the Si surface with the hydrophilic alkyl groups pointing away from the surface lowers γ_{SG}. Since IPA vapor rather decreases γ_{LG},[26] it should be overcompensated by the decrease in $\gamma_{SG} - \gamma_{SL}$. We also note that uneven evaporation rates near the contact line of sessile drops give rise to internal convection,[34,35] which will tend to suppress the change of γ_{LG} and γ_{SL} due to IPA vapor. Therefore, we attribute the rapid increase in θ before the plateau to mainly the decrease in γ_{SG} by the adsorption of IPA vapor molecules on the solid surface. The contact angle slowly falls when the sessile drops are exposed to IPA for over 100 s due to the eventual decrease in γ_{LG} caused by the volumetric mixing of IPA with water drops. However, the time scale of our interest in film dewetting, ~1 s, implies that the film dynamics investigated in this work is dominated by the decrease in γ_{SG}.

Solving the diffusion equation for c in the air surrounding the overhanging IPA drop, as shown in Fig. 1(a), we find $c/c_s \approx a/r_b \sim 0.1$ on the exposed dry hole.[26] Figure 4(d) indicates that the contact angle of the IPA-adsorbed solid under such a concentration of IPA is $\theta \approx \theta_m$. Young's equation then allows us to write $\gamma_{SG} - \gamma_{SL} = \gamma_0 \cos\theta_m$.

REFERENCES

[1] P.-G. de Gennes, F. Brochard-Wyart, and D. Quéré, *Capillarity and Wetting Phenomena: Drops, Bubbles, Pearls, Waves* (Springer, 2004).
[2] G. I. Taylor, "The dynamics of thin sheets of fluid. III. Disintegration of fluid sheets," Proc. R. Soc. London, Ser. A **253**, 313–321 (1959).
[3] F. E. C. Culick, "Comments on a ruptured soap film," J. Appl. Phys. **31**, 1128–1129 (1960).
[4] S. Kim, M.-W. Moon, and H.-Y. Kim, "Drop impact on super-wettability-contrast annular patterns," J. Fluid Mech. **730**, 328–342 (2013).
[5] C. Redon, J. B. Brzoska, and F. Brochard-Wyart, "Dewetting and slippage of microscopic polymer films," Macromolecules **27**, 468–471 (1994).
[6] G. Reiter and R. Khanna, "Real-time determination of the slippage length in autophobic polymer dewetting," Phys. Rev. Lett. **85**, 2753–2756 (2000).
[7] C. W. J. Berendsen, J. C. H. Zeegers, G. C. F. L. Kruis, M. Riepen, and A. A. Darhuber, "Rupture of thin liquid films induced by impinging air-jets," Langmuir **28**, 9977 (2012).
[8] O. E. Jensen and J. B. Grotberg, "Insoluble surfactant spreading on a thin viscous film: Shock evolution and film rupture," J. Fluid Mech. **240**, 259–288 (1992).
[9] M. R. E. Warner, R. V. Craster, and O. K. Matar, "Fingering phenomena associated with insoluble surfactant spreading on thin liquid films," J. Fluid Mech. **510**, 169–200 (2004).
[10] J. H. Hernandez-Sanchez, A. Eddi, and J. H. Snoeijer, "Marangoni spreading due to a localized alcohol supply on a thin water film," Phys. Fluids **27**, 032003 (2015).
[11] L. Keiser, H. Bense, P. Colinet, J. Bico, and E. Reyssat, "Marangoni bursting: Evaporation-induced emulsification of binary mixtures on a liquid layer," Phys. Rev. Lett. **118**, 074504 (2017).
[12] D. H. Bangham and Z. Saweris, "The behaviour of liquid drops and adsorbed films at cleavage surfaces of mica," Trans. Faraday Soc. **34**, 554–570 (1938).
[13] P. Carles and A. M. Cazabat, "Spreading involving the Marangoni effect: Some preliminary results," Colloids Surf. **41**, 97–105 (1989).

[14]P. Bahadur, P. S. Yadav, K. Chaurasia, A. Leh, and R. Tadmor, "Chasing drops: Following escaper and pursuer drop couple system," J. Colloid Interface Sci. **332**, 455–460 (2009).
[15]M. Sellier, V. Nock, C. Gaubert, and C. Verdier, "Droplet actuation induced by coalescence: Experimental evidences and phenomenological modeling," Eur. Phys. J.: Spec. Top. **219**, 131–141 (2013).
[16]N. J. Cira, A. Benusiglio, and M. Prakash, "Vapour-mediated sensing and motility in two-component droplets," Nature **519**, 446–450 (2015).
[17]M. Majumder, C. S. Rendall, J. A. Eukel, J. Y. L. Wang, N. Behabtu, C. L. Pint, T.-Y. Liu, A. W. Orbaek, F. Mirri, J. Nam, A. R. Barron, R. H. Hauge, H. K. Schmidt, and M. Pasquali, "Overcoming the "coffee-stain" effect by compositional Marangoni-flow-assisted drop-drying," J. Phys. Chem. B **116**, 6536–6542 (2012).
[18]O. Hegde, S. Chakraborty, P. Kabi, and S. Basu, "Vapor mediated control of microscale flow in sessile droplets," Phys. Fluids **30**, 122103 (2018).
[19]R. Malinowski, G. Volpe, I. P. Parkin, and G. Volpe, "Dynamic control of particle deposition in evaporating droplets by an external point source of vapor," J. Phys. Chem. Lett. **9**, 659–664 (2018).
[20]B. Néel and E. Villermaux, "The spontaneous puncture of thick liquid films," J. Fluid Mech. **838**, 192–221 (2018).
[21]S. Karpitschka, F. Liebig, and H. Riegler, "Marangoni contraction of evaporating sessile droplets of binary mixtures," Langmuir **33**, 4682–4687 (2017).
[22]A. F. M. Leenaars, J. A. M. Huethorst, and J. J. van Oekel, "Marangoni drying: A new extremely clean drying process," Langmuir **6**, 1701–1703 (1990).
[23]J. Marra and J. A. M. Huethorst, "Physical principles of Marangoni drying," Langmuir **7**, 2748–2755 (1991).
[24]O. K. Matar and R. V. Craster, "Models for Marangoni drying," Phys. Fluids **13**, 1869–1883 (2001).
[25]C. Li, D. Zhao, J. Wen, J. Cheng, and X. Lu, "Evolution of entrained water film thickness and dynamics of Marangoni flow in Marangoni drying," RSC Adv. **8**, 4995–5004 (2018).
[26]S. Kim, J. Kim, and H.-Y. Kim, "Dewetting of liquid film via vapour-mediated Marangoni effect," J. Fluid Mech. **872**, 100–114 (2019).
[27]G. K. Batchelor, *An Introduction to Fluid Dynamics* (Cambridge University Press, 1967).
[28]H.-Y. Kim, "On thermocapillary propulsion of microliquid slug," Nanoscale Microscale Thermophys. Eng. **11**, 351–362 (2007).
[29]H. S. Carslaw and J. C. Jaeger, *Conduction of Heat in Solids* (Clarendon Press, 1959).
[30]G. A. Lugg, "Diffusion coefficients of some organic and other vapors in air," Anal. Chem. **40**, 1072–1077 (1968).
[31]J. N. Israelachvili, *Intermolecular and Surface Forces*, 3rd ed. (Elsevier, 2011).
[32]J. Liu and P. Zuo, "Wetting and elasto-plasticity based sculpture of liquid marbles," Eur. Phys. J. E **39**, 17 (2016).
[33]M. Lee, Y. S. Chang, and H.-Y. Kim, "Drop impact on microwetting patterned surfaces," Phys. Fluids **22**, 072101 (2010).
[34]R. D. Deegan, O. Bakajin, T. F. Dupont, G. Huber, S. R. Nagel, and T. A. Witten, "Capillary flow as the cause of ring stains from dried liquid drops," Nature **389**, 827–829 (1997).
[35]T. V. Kasyap, D. L. Koch, and M. Wu, "Bacterial collective motion near the contact line of an evaporating sessile drop," Phys. Fluids **26**, 111703 (2014).